Journal of Luminescence 51 (1992) 297–314
North-Holland

JOURNAL OF
LUMINESCENCE

Intersystem-crossing and excited-state absorption in eosin Y solutions determined by picosecond double pulse transient absorption measurements

A. Penzkofer, A. Beidoun and M. Daiber

Naturwissenschaftliche Fakultät II-Physik, Universität Regensburg, W-8400 Regensburg, Germany

Received 17 July 1991
Revised 25 November 1991
Accepted 25 November 1991

The transmission measurement of two intense picosecond pulses (wavelength $\lambda_L = 527$ nm) separated by 10 ns is applied to extract the quantum yield of triplet formation ϕ_T, the S_1 singlet excited state absorption cross-section σ_{ex}, the T_1 triplet absorption cross-section σ_T, and the T_n–T_1 relaxation time τ_T in the triplet system. Additionally the fluorescence quantum yields ϕ_F are measured with a spectrofluorimeter. For eosin Y in water the determined data are $\phi_T \approx 0.8$, $\phi_F \approx 0.2$, $\sigma_{ex} \approx 4.5\times10^{-17}$ cm^2, $\sigma_T \approx 5.5\times10^{-17}$ cm^2, and $\tau_T \approx 1$ ps. The data for eosin Y in methanol are $\phi_T \approx 0.56$, $\phi_F \approx 0.44$, $\sigma_{ex} \approx 3\times10^{-17}$ cm^2, $\sigma_T \approx 4.9\times10^{-17}$ cm^2, and $\tau_T \approx 1$ ps.

1. Introduction

Eosin Y (the disodium salt of 2′,4′,5′,7′-tetrabromofluorescein, structural formula is shown in fig. 5) is an important stain in histology [1,2]. It is applied as a photo-oxidation sensitizer due to its high efficiency of singlet oxygen generation [3–6]. Laser action of eosin Y was achieved in various solvents [7–12]. The dye was applied to nonlinear optical processes like low power phase conjugation [13–15] and spatial light modulation [16].

Triplet spectroscopic data of eosin Y are collected in refs. [17,18]. An enhanced intersystem crossing occurs due to the heavy atom effect of Br [19,20]. Phosphorescence [21] and delayed fluorescence [22,23] have been observed even at room temperature. Reported values of the quantum yield of triplet formation ϕ_T and of the fluorescence quantum yield ϕ_F are listed in table 1. In early studies small quantum yields of triplet formation were deduced while in more recent reports the nonradiative relaxation was found to be completely due to intersystem crossing.

The quantum yields of triplet formation or the intersystem-crossing rates for eosin Y have been deduced from phosphorescence quantum yield and phosphorescence lifetime measurements in a spectrophosphorimeter [22], from sensitized photoreduction studies [24,25], and from absorption measurements using microsecond flash photolysis systems [26–28], a pulsed submicrosecond dye laser [29], and a repetitive subnanosecond dye laser [30].

In this paper we determine the quantum yield of triplet formation ϕ_T, the S_1–S_n singlet state absorption cross-section $\sigma_{ex}(\lambda_L)$, the T_1–T_n triplet–triplet absorption cross-section $\sigma_T(\lambda_L)$, and the

Correspondence to: A. Penzkofer, Naturwissenschaftliche Fakultät II-Physik, Universität Regensburg, W-8400 Regensburg, Germany.

0022-2313/92/$05.00 © 1992 – Elsevier Science Publishers B.V. All rights reserved

Table 1
Quantum yields of triplet formation ϕ_T and of fluorescence ϕ_F for eosin Y at room temperature.

Solvent	H_2O	Methanol	Ethanol	Glycerol
ϕ_T	0.092 [25]	0.18 [27,45] [b]	0.021 [22]	0.036 [22]
	0.71 [26]	0.25 [27,67] [b]	0.43 [24]	
	0.76 [29]	0.56 ± 0.07 [a]	0.33 [27,45] [c]	
	0.64 [66]		0.34 [30]	
	0.8 ± 0.08 [a]			
ϕ_F	0.15 [68]	0.63 [27,45]	0.40 [68]	0.45 [22]
	0.19 [26]	0.60 [48]	0.72 [22]	
	0.20 [48]	0.49 [12]	0.67 [46]	
	0.22 [22]	0.44 ± 0.04 [a]	0.69 [48]	
	0.20 [69]			
	0.20 ± 0.02 [a]			

[a] this work.
[b] calculated from reported k_{isc} values by using eq. (14) and $\tau_{S1} = 2$ ns (table 2).
[c] calculated from reported k_{isc} value by using eq. (14) and $\tau_{S1} = 3.62$ ns [48].

T_n–T_1 triplet relaxation time τ_T of eosin Y in bidistilled water (pH ≈ 7) and in absolute methanol by nonlinear transmission measurements with a sequence of two second harmonic picosecond light pulses of a mode-locked Nd:glass laser (pulse separation $t_R = 10$ ns, excitation wavelength $\lambda_L = 527$ nm). Our studies give quantum yields of triplet formation of $\phi_T(\text{water}) = 0.8 \pm 0.08$ and $\phi_T(\text{methanol}) = 0.56 \pm 0.07$. Additionally the fluorescence quantum yields ϕ_F are determined by conventional spectro-fluorimetry. The obtained fluorescence quantum efficiences are $\phi_F(H_2O) = 0.2 \pm 0.02$ and $\phi_F(\text{methanol}) = 0.44 \pm 0.04$. These data give quantum yields of internal conversion $\phi_{ic}(H_2O) \leqslant 0.1$ and $\phi_{ic}(\text{methanol}) \leqslant 0.11$.

2. Method

The relevant level diagram for the absorption and emission dynamics of eosin Y is displayed in fig. 1(a). A schematic of the applied double-pulse pump and probe experimental arrangement is shown in fig. 1(b).

The picosecond pulses L1 and L2 (duration $\Delta t_L \simeq 5$ ps, separation $t_R = 10$ ns) excite molecules from the S_0 ground state to a Franck–Condon level 2 in the first excited singlet band S_1. From there the molecules thermalize within the S_1-band (time constant τ_{FC}) to level 3. From the levels 2 and 3 there occurs excitation to higher singlet states S_n (level 4, excited state absorption cross-section σ_{ex}), radiative relaxation (level 7, spontaneous emission, radiative lifetime τ_{rad}) and internal conversion (rate constant k_{ic}) to the ground state (level 1), as well as intersystem-crossing to the triplet system (level 5, rate constant k_{isc}). The spontaneous emission may be enhanced by stimulated emission (amplified spontaneous emission [31,32]). In the triplet system the laser light causes T_1–T_n triplet–triplet absorption (excitation to level 6, absorption cross-section σ_T). The excited molecules in the levels 4 and 6 relax with time constants τ_{ex} and τ_T, respectively. The molecules in the triplet system return slowly to the S_0 ground state with the phosphorescence lifetime τ_P.

For the special situation of eosin Y in H_2O levels 2 and 3 coincide practically (laser frequency ν_L is equal to pure electronic S_0–S_1 transition frequency ν_{S1}), and for the solvent methanol level 2 is only slightly above level 3 causing a thermal population $N_{2,th}$ of level 2 in the S_1-band.

The temporal population changes of the molecular levels and the transmission changes caused by the double pump pulse bleaching experiments are illustrated in figs. 2 and 3. The small population and transmission changes caused by the weak delayed probe pulses are neglected.

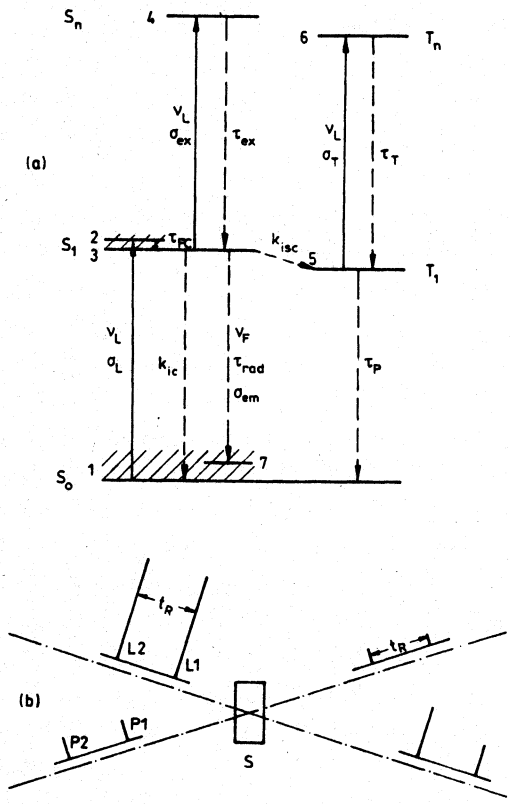

Fig. 1. (a) Energy level diagram of eosin Y. (b) Schematic of pump and probe double pulse propagation through sample.

In fig. 2 the situation of $k_{isc} = 0$ (no triplet population) is shown. The S_1-state lifetime (fluorescence lifetime) τ_{S1} is long compared to the laser pulse duration ($\Delta t_L \simeq 5$ ps) and short compared to the double pulse separation t_R (= 10 ns) or the probe pulse delay t_D (≈ 8 ns). The system relaxes completely before interrogating with the delayed probe pulses or the second pump pulse. The triplet levels 5 and 6 are not populated (population number densities $N_5 = N_6 = 0$). The double pulses have equal transmissions, i.e. $T_{L1} = T_{L2}$ and $T_{P1} = T_{P2}$.

The situation of $k_{isc} \neq 0$ (quantum yield of triplet population $\phi_T > 0$) is shown schematically in fig. 3. The ground-state population N_1 does not recover completely because of triplet-state population. The S_1-state level population N_3 caused by the second pump pulse is smaller than its population caused by the first pump pulse because the ground-state population has decreased. The population accumulation N_5 in the lowest triplet state T_1 is seen in fig. 3(f). The T_1 level depletion by the second pump pulse L2 and the fast level refilling by T_n–T_1 triplet–triplet relaxation τ_T are indicated (fig. 3(f) and (g)). The time dependent light transmission is illustrated in fig. 3(h) for the cases of $\sigma_T = 0$ (dashed curve), $\sigma_T < \sigma_L$ (solid curve), $\sigma_T = \sigma_L$ (dotted curve), and $\sigma_T > \sigma_L$ (dash-dotted curve). For $\sigma_T \neq 0$ the transmission peak at $t = t_R$ is due to triplet absorption bleaching and triplet absorption recovery (short value of τ_T).

The transmission T_{L1} of the first pump pulse L1 is independent of triplet state absorption data because the population of the triplet state within the duration of the pump pulse is too small. The intensity dependent measurement of T_{L1} allows the determination of the S_1–S_n singlet–singlet excited state absorption cross-section σ_{ex}.

The transmission T_{L2} of the second pump pulse L_2 depends, additionally to the singlet absorption cross-sections σ_L and σ_{ex}, on the quantum yield of triplet formation ϕ_T(proportional to k_{isc}, see below),

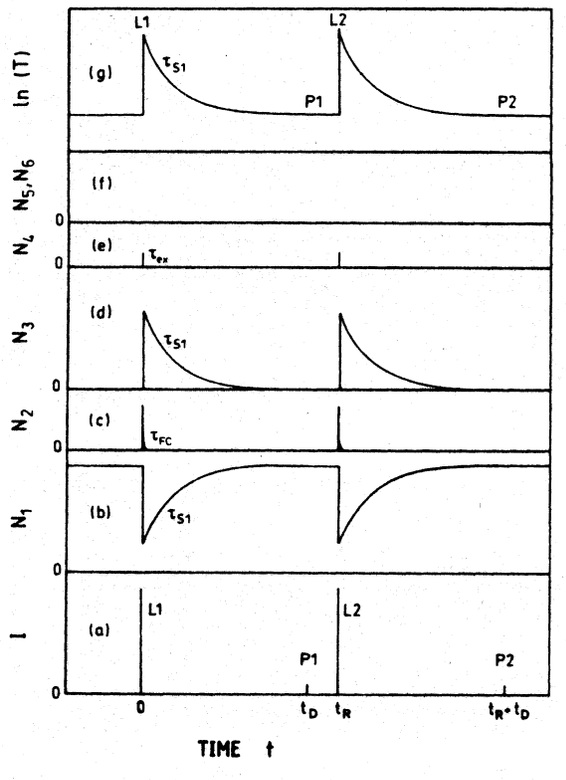

Fig. 2. Schematic of population and transmission dynamics of dye due to double excitation in the case of no intersystem-crossing ($k_{isc} = 0$, $\phi_T = 0$). (a) Pulse sequence. (b–f) level populations. (g) Temporal transmission.

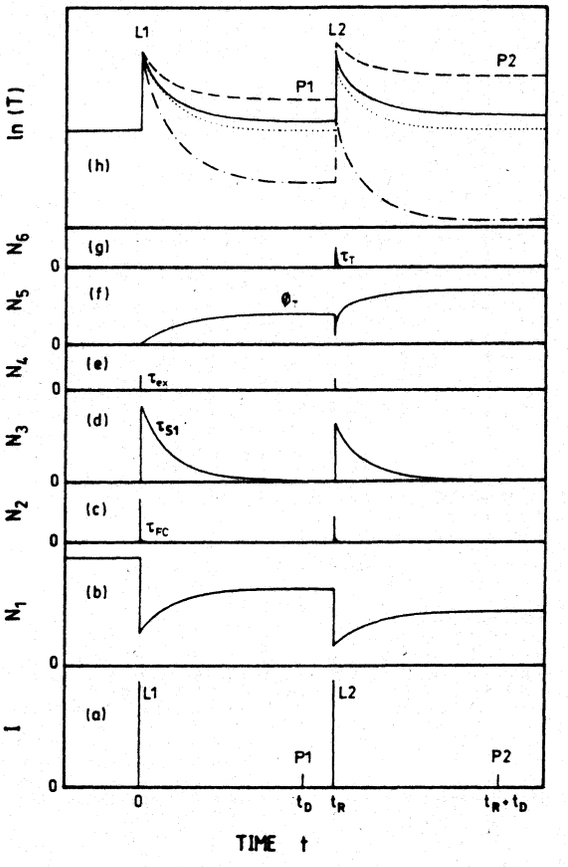

Fig. 3. Schematic of population and transmission dynamics of dye due to double pulse excitation in the case of intersystem-crossing ($k_{isc} > 0$, $\phi_T > 0$). (a) Pulse sequence. (b–g) Level populations. (h) Temporal transmission for $\sigma_T = 0$ (dashed curve), $0 < \sigma_T < \sigma_L$ (solid curve), $\sigma_T = \sigma_L$ (dotted curve), $\sigma_T > \sigma_L$ (dash-dotted curve).

the triplet–triplet absorption cross-section σ_T, and the triplet relaxation time τ_T. The measurement of T_{L2} over a wide pump intensity region I_{L2} allows the determination of the three parameters ϕ_T, σ_T, and τ_T by comparison of the experimental transmission values with numerically simulated transmission curves (see below).

The delayed probe pulse transmissions T_{P1} and T_{P2} ($\tau_F \ll t_D < t_R$) are given by $T_{P1} = \exp[-N_1(t_D)\sigma_L l - N_5(t_D)\sigma_T l] = T_0 \exp[(\sigma_L - \sigma_T)N_5(t_D)l]$, and $T_{P2} = T_0 \exp[(\sigma_L - \sigma_T)N_5(t_D + t_R)l]$, where l is the sample length and T_0 is the transmission of the unexcited dye sample (see below). The value of T_{P1} indicates only whether $\sigma_T < \sigma_L$ (then $T_{P1} > T_0$) or $\sigma_T > \sigma_L$ (then $T_{P1} < T_0$). T_{P2} depends additionally on the triplet relaxation time τ_T (see below).

All relevant parameters are already determined by measuring T_{L1} and T_{L2} over a wide pump intensity range $I_L = I_{L1} = I_{L2}$. The S_1-state lifetime τ_{S1} has to be determined separately, for example by fluorescence quantum yield measurements as is done in this work. It is not necessary to measure the transmission of the delayed probe pulses. In this work they are measured to confirm the results of the pump pulse transmission measurements.

3. Theory

The saturable absorption dynamics of the two pump pulses and the transient absorption of the two probe pulses is described by the following differential equation system for the level population number densities N_1–N_6 and the pulse intensities I_{L1}, L_{L2}, I_{P1}, and I_{P2} [31]:

$$\frac{\partial N_1(\theta)}{\partial t'} = -3\sigma_L \cos^2\theta\left[N_1(\theta) - N_2(\theta)\right]\frac{I_{L1}+I_{L2}}{h\nu_L} + \left[N_2(\theta)+N_3(\theta)\right]\left(\tau_{rad}^{-1}+k_{ic}\right) + \frac{N_5(\theta)}{\tau_P} - \frac{N_1(\theta)-\bar{N}_1}{\tau_{or,S0}}, \tag{1}$$

$$\frac{\partial N_2(\theta)}{\partial t'} = \left\{3\sigma_L \cos^2\theta\left[N_1(\theta)-N_2(\theta)\right] - \sigma_{ex}\left[N_2(\theta) - \frac{N_2(\theta)}{N_2(\theta)+N_3(\theta)}N_4(\theta)\right]\right\}\frac{I_{L1}+I_{L2}}{h\nu_L} - \frac{N_2(\theta)-N_{2,th}(\theta)}{\tau_{FC}} - \frac{N_2(\theta)}{\tau_{S1}} - k_{isc}N_2(\theta) - \frac{N_2(\theta)-\bar{N}_2}{\tau_{or,S1}}, \tag{2}$$

$$\frac{\partial N_3(\theta)}{\partial t'} = \frac{N_2(\theta)-N_{2,th}(\theta)}{\tau_{FC}} - \sigma_{ex}\left[N_3(\theta) - \frac{N_3(\theta)}{N_2(\theta)+N_3(\theta)}N_4(\theta)\right]\frac{I_{L1}+I_{L2}}{h\nu_L} + \frac{N_4(\theta)}{\tau_{ex}} - \frac{N_3(\theta)}{\tau_{S1}} - k_{isc}N_3(\theta) - \frac{N_3(\theta)-\bar{N}_3}{\tau_{or,S1}}, \tag{3}$$

$$\frac{\partial N_4(\theta)}{\partial t'} = \sigma_{ex}\left[N_2(\theta)+N_3(\theta)-N_4(\theta)\right]\frac{I_{L1}+I_{L2}}{h\nu_L} - \frac{N_4(\theta)}{\tau_{ex}} - \frac{N_4(\theta)-\bar{N}_4}{\tau_{or,Sn}}, \tag{4}$$

$$\frac{\partial N_5(\theta)}{\partial t'} = k_{isc}\left[N_2(\theta)+N_3(\theta)\right] - 3\sigma_T \cos^2\theta\left[N_5(\theta)-N_6(\theta)\right]\frac{I_{L1}+I_{L2}}{h\nu_L} + \frac{N_6(\theta)}{\tau_T} - \frac{N_5(\theta)}{\tau_P} - \frac{N_5(\theta)-\bar{N}_5}{\tau_{or,T1}}, \tag{5}$$

$$\frac{\partial N_6(\theta)}{\partial t'} = 3\sigma_T \cos^2\theta\left[N_5(\theta)-N_6(\theta)\right]\frac{I_{L1}+I_{L2}}{h\nu_L} - \frac{N_6(\theta)}{\tau_T} - \frac{N_6(\theta)-\bar{N}_6}{\tau_{or,Tn}}, \tag{6}$$

$$\frac{\partial I_{Li}}{\partial z'} = -3\sigma_L I_{Li}\int_0^{\pi/2}\left[N_1(\theta)-N_2(\theta)\right]\cos^2\theta\sin\theta\,d\theta - \sigma_{ex}I_{Li}\left(\bar{N}_2+\bar{N}_3\right) - 3\sigma_T I_{Li}\int_0^{\pi/2}N_5(\theta)\cos^2\theta\sin\theta\,d\theta, \quad i=1,2, \tag{7}$$

$$\frac{\partial I_{Pi}}{\partial z'} = -I_{Pi}\left[\sigma_L\left(\bar{N}_1-\bar{N}_2\right)+\sigma_{ex}\left(\bar{N}_2+\bar{N}_3\right)+\sigma_T\bar{N}_5\right] \approx -I_{Pi}\left(\sigma_L\bar{N}_1+\sigma_T\bar{N}_5\right) = -I_{Pi}\left[\sigma_L N_0-(\sigma_L-\sigma_T)\bar{N}_5\right], \quad i=1,2, \tag{8}$$

$$\bar{N}_i = \int_0^{\pi/2}N_i(\theta)\sin\theta\,d\theta, \quad i=1,\ldots,6, \tag{9}$$

$$N_{2,th}(\theta) = N_3(\theta)\exp(-h\,\Delta\nu_{23}/k_B\vartheta), \tag{10}$$

$$T_{E,i} = \frac{\int_0^\infty r\int_{-\infty}^{\infty}I_i(t',l,r)\,dt'\,dr}{\int_0^\infty r\int_{-\infty}^{\infty}I_i(t',0,r)\,dt'\,dr}, \quad i=\text{L1,L2,P1,P2}. \tag{11}$$

The transformation $t' = t - c_0 z/n$ and $z' = z$ used, where t is the time, z is the distance along the propagation direction, c_0 is the light velocity in vacuum, and n is the refractive index. l is the sample length.

The absorption anisotropy of the electric dipole interaction causes an angular anisotropic level population. The orientational anisotropic distributions relax to isotropic distributions with the molecular reorientation time constants τ_{or}, $(i = S_0, S_1, S_n, T_1, T_n)$. In the calculations the various $\tau_{or,i}$ are set to a single parameter τ_{or}. $\bar{N}_i$, $i = 1,\ldots,6$, are the orientation averaged level populations. For the S_0–S_1 ground-state absorption of the pump pulses L1 and L2 the absorption anisotropy is taken into account by the angle dependent absorption cross-section $\sigma_L(\theta) = 3\sigma_L \cos^2\theta$, where θ is the angle between the S_0–S_1 transition dipole moment of the molecules and the direction of the electric field of the linearly polarized laser light. For the S_1–S_n excited state absorption of the pump pulses L1 and L2 an isotropic absorption dynamics is used in the equation system since the relative orientation between S_0–S_1 transition dipole moments and the S_1–S_n transition dipole moments is unknown. At high pump intensities the S_1-level populations $N_2(\theta)$ and $N_3(\theta)$ approach the isotropic distribution $\bar{N}_2$ and $\bar{N}_3$ because of nearly complete depletion of the ground-state population N_1. Therefore the isotropic excited singlet state absorption approach gives correct excited state absorption cross-sections σ_{ex}. The first pump pulse L1 does not suffer triplet absorption since the pump pulse duration is very short compared to the inverse intersystem crossing rate, i.e. $\Delta t_L \ll k_{isc}^{-1}$. The absorption of pump pulse L2 starts from an isotropic triplet T_1 level population N_5 because $\tau_{or} \ll t_R$. This fact allows to take the absorption anisotropy of the triplet–triplet absorption into account by $\sigma_T(\theta) = 3\sigma_T \cos^2\theta$, where θ is the angle between the T_1–T_n transition dipole moment of the molecules and the direction of the electric field strength of the laser light. The delayed probe pulses P1 and P2 suffer only isotropic absorption since $\tau_{or} \ll t_D$.

The coincidence of the levels 2 and 3 ($\Delta\nu_{23} = \nu_2 - \nu_3 \simeq 0$) in the case of eosin Y in H_2O and the thermal population of level 2 ($N_{2,th}$) in the case of eosin Y in methanol is taken into consideration in eqs. (2) and (3) by the term $[N_2(\theta) - N_{2,th}]/\tau_{FC}$. $N_{2,th}$ is given by eq. (10) where $\Delta\nu_{23}$ is the frequency difference between the levels 2 and 3, h is the Planck constant, k_B is the Boltzmann constant, and ϑ is the temperature.

The S_1-state relaxation time τ_{S1} is determined by the radiative relaxation time τ_{rad}, the internal conversion rate k_{ic} and the intersystem crossing rate k_{isc} according to

$$\tau_{S1}^{-1} = \tau_{rad}^{-1} + k_{ic} + k_{isc}, \tag{12}$$

as long as the S_1-state lifetime shortening by amplified spontaneous emission [31,32] is negligible (see below). Under this condition τ_{S1} is related to the fluorescence quantum yield ϕ_F by

$$\tau_{S1} = \phi_F \tau_{rad}. \tag{13}$$

The intersystem crossing rate is related to the quantum yield of triplet formation ϕ_T by

$$k_{isc} = \phi_T/\tau_{S1}. \tag{14}$$

Inserting eqs. (13) and (14) into eq. (12) allows us to express the internal conversion rate as

$$k_{ic} = \frac{1 - \phi_F - \phi_T}{\tau_{S1}}. \tag{15}$$

The quantum yield of internal conversion is $\phi_{ic} = 1 - \phi_F - \phi_T$.

The initial conditions of the level populations are $N_1(\theta, t' = -\infty, z', r) = N_0$ and $N_i(\theta, t' = -\infty, z', r) = 0$ for $i = 2,\ldots,6$. N_0 is the total number density of dissolved dye molecules. The input pulse intensities are

$$I_{L1}(t', z' = 0, r) = I_{0L1} \exp\left[-\left(\frac{t'}{t_0}\right)^2 - \left(\frac{r}{r_L}\right)^2\right], \tag{16a}$$

$$I_{L2}(t',z'=0,r)=I_{0L2}\exp\left[-\left(\frac{t'-t_R}{t_0}\right)^2-\left(\frac{r}{r_L}\right)^2\right], \tag{16b}$$

$$I_{P1}(t',z'=0,r)=I_{0P1}\exp\left[-\left(\frac{t'-t_D}{t_0}\right)^2-\left(\frac{r}{r_P}\right)^2\right], \tag{16c}$$

$$I_{P2}(t',z'=0,r)=I_{0P2}\exp\left[-\left(\frac{t'-t_D-t_R}{t_0}\right)^2-\left(\frac{r}{r_P}\right)^2\right]. \tag{16d}$$

r is the radial laser beam coordinate. r_L and r_P are the $1/e$ beam radii of the pump and the probe pulses, respectively ($r_L \approx r_P$ in experiment, $r_L = r_P$ used in calculations). $t_0 = 2^{-1}[\ln(2)]^{-1}\Delta t_L$ is half the $1/e$ temporal pulse width (Δt_L is the FWHM pulse duration). t_R is the temporal separation of the double pulses, and t_D is the temporal delay of the probe pulse sequence from the pump pulse sequence.

The equation system (1)–(8) is solved numerically using relevant parameters of eosin Y. The unknown parameters σ_{ex}, ϕ_T, σ_T, and τ_T are varied and determined by fitting the calculated energy transmission curves to the experimental energy transmission values.

In the equation system (1)–(8) the amplification of spontaneous emission [31,32] is neglected. An efficient amplification of the spontaneous emission at frequency ν_F by stimulated emission with cross-section σ_{em} (see fig. 1(a)) would shorten the S_1-state lifetime τ_{S1} to τ_{ASE} and thereby influence the quantum yield of triplet formation ϕ_T. In our studies the experimental parameters have been chosen in such a way that τ_{ASE} is nearly equal to τ_{S1}. Otherwise it would be necessary to include the dynamics of amplified spontaneous emission [31,32] in the equation system for the saturable absorption dynamics.

In ref. [32] a relation between τ_{ASE} and τ_{S1} was derived (eq. (43) there). It reads

$$\tau_{ASE}=\frac{\tau_{S1}}{1+\dfrac{q_F\Delta\Omega\sigma_{em}}{4\pi(\sigma_{em}-\sigma_{ex,F})}\left\{\exp\left[(\sigma_{em}-\sigma_{ex,F})N_3(\bar{t},\bar{z})l\right]-1\right\}} \tag{17a}$$

$$\approx\frac{\tau_{S1}}{1+\dfrac{q_F\Delta\Omega}{4\pi}\left[\left(\dfrac{T_{E,L1}}{T_0}\right)^{(\sigma_{em}-\sigma_{ex,F})/(\sigma_L-\sigma_{ex})}-1\right]}. \tag{17b}$$

In eq. 17(a) is $\bar{t}\approx\Delta t_L$ and $\bar{z}\approx l/2$, $\sigma_{ex,F}$ is the S_1–S_n excited state absorption at frequency ν_F, and $\Delta\Omega\approx\pi d_L^2/(4l^2)$ is the solid angle of the amplified spontaneous emission (d_L is pump laser beam diameter, l is sample length). The approximation (17(b)) is obtained by setting $N_3(\bar{t},\bar{z})\approx\ln(T_{E,L1}/T_0)/[(\sigma_L-\sigma_{ex})l]$. The condition $\tau_{ASE}\approx\tau_{S1}$ may be fulfilled experimentally by limiting $T_{E,L1}/T_0$ and by making the value of $\Delta\Omega$ small ($l\gg d_L$).

4. Experimental

4.1. Experimental set-up for picosecond double pulse absorption measurements

The experimental set-up is shown in fig. 4. A train of picosecond light pulses is generated in an active and passive mode-locked pulsed Nd:phosphate glass laser [34]. The laser shot repetition rate is approximately 0.05 Hz. Two adjacent pulses are separated from the pulse train with a Kerr cell shutter activated by a laser triggered spark gap [35]. (Coaxial charging cable between spark gap and high Ohmic

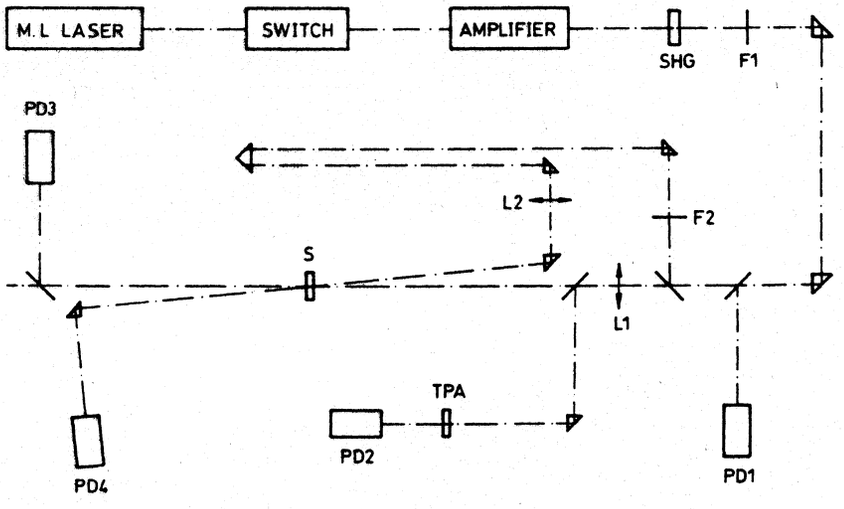

Fig. 4. Picosecond double pulse transient absorption measurement arrangement. SHG, CDA crystal for second harmonic generation, F1, F2, filters. L1, L2, lenses. TPA, two-photon absorbing rutile crystal for peak intensity detection. PD1-PD4, photodetectors. S, sample.

resistor is ca. 1.7 m long causing a high voltage pulse of approximately 17 ns duration on the Kerr cell after spark gap triggering. Kerr liquid is nitrobenzene.) The separated pulse pairs are increased in energy in a Nd:phosphate glass amplifier. The second harmonic of the pulses [36] is generated in a noncritical 90° phase-matched CDA crystal [34] (cesium dihydrogen arsenate CsH_2AsO_4, phase-matching temperature 34°C, crystal length 1 cm). After the CDA crystal the fundamental laser light is filtered out by a short-pass edge filter F1. The parameters of the second harmonic light pulses are: wavelength $\lambda_L = 527$ nm, pulse duration $\Delta t_L \simeq 5$ ps (FWHM), pulse separation $t_R = 10$ ns (resonator round-trip time), and pulse energy up to 2 mJ. The peak intensities I_{0L1} and I_{0L2} of the two pump pulses are determined by energy transmission measurements through a two-photon absorbing rutile crystal [38] (photodetectors PD1 and PD2). The laser peak intensities I_{0L1} and I_{0L2} are varied either by removing lens L1 and varying the pump voltage of the Nd:glass laser amplifier (for low intensities) or by inserting lenses L1 of different focal lengths in the light path (for high intensities). The laser beam diameter without lens narrowing was $d_L \approx 1.5$ mm. The sample lengths were $l = 2$ mm for eosin Y in H_2O and $l = 1$ cm for eosin Y in methanol. The energy transmissions $T_{E,L1}$ and $T_{E,L2}$ of the pump pulses through the sample S are measured with the photodetectors PD3 and PD1. The probe pulses are separated by a beam splitter and pass through the excitation region of the sample at a temporal delay of $t_D = 8$ ns ($< t_R = 10$ ns, $t_D \gg \tau_{S1}$) relative to the pump pulses. The probe pulse energy transmissions $T_{E,P1}$ and $T_{E,P2}$ are measured with the photodetectors PD4 and PD1. The transmissions $T_{E,L1}$, $t_{E,L2}$, $T_{E,P1}$ and $T_{E,P2}$ are determined for each single laser shot. For each data point presented in the figs. 8 to 11 approximately 10 individual points were grouped and averaged.

4.2. Determination of steady-state absorption and fluorescence spectra

The absorption cross-section spectra are determined by transmission measurements with a conventional spectrophotometer (Beckman model ACTA MIV).

The fluorescence quantum distribution spectra $E(\lambda)$ [39] are determined with a homebuilt spectro-fluorimeter. The multi-line emission of an argon ion laser is used as the excitation source. The fluorescence is collected at right angles to the excitation light propagation direction. A polarizer is inserted in the

fluorescence path for magic angle polarization detection [40] (vertically polarized argon ion laser, polarizer in the fluorescence path at an angle of 54.7° to the vertical direction). A monochromator is scanned over the fluorescence wavelength region. The fluorescence signal is detected with a microchannel plate photomultiplier tube (Hamamatsu type R-1564-01). Rhodamine 6G in ethanol was employed for the spectral fluorescence standard ($\phi_F = 0.95$ [41]). A halogen–tungsten lamp (Osram type HLX 64655) of known colour temperature (3450 K at 12 V voltage) was applied for spectral sensitivity calibration [42].

The fluorescence quantum yields ϕ_F are obtained by integration over the fluorescence quantum distribution spectra ($\phi_F = \int_{em} E(\lambda)\, d\lambda$) [39]. The radiative lifetimes τ_{rad} are determined by application of the Strickler–Berg formula [43,44] (for reported τ_{rad} data of eosin Y see refs. [11,45–48]). The fluorescence lifetime τ_{S1} is given by eq. (13). The stimulated emission cross-section spectra are calculated from the fluorescence quantum distribution spectra $E(\lambda)$, and the radiative lifetimes τ_{rad} [49,50]. The pure electronic S_0–S_1 transition frequency ν_{S1} is determined by the crossing of the $\sigma_{abs}(\lambda)$ and $\sigma_{em}(\lambda)$ curves [$\sigma_{abs}(\nu_{S1}) = \sigma_{em}(\nu_{S1})$].

4.3. Dye preparation

Eosin Y was purchased from Heraeus. The structural formula of the molecule is included in fig. 5 (molecular mass 691.88 g/mol). The dye was purified by recrystallization six times from ethanol [24,51,52].

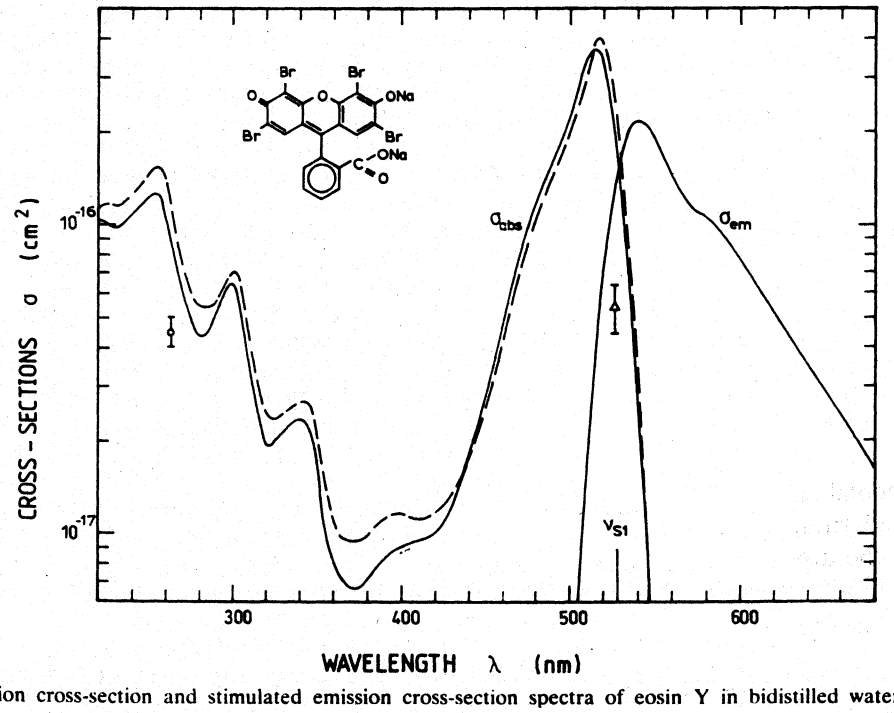

Fig. 5. Absorption cross-section and stimulated emission cross-section spectra of eosin Y in bidistilled water. Dashed curve, absorption cross-section spectrum of chromatographically purified eosin Y in H_2O (from ref. [53]). The circle indicates the determined S_1–S_n excited state absorption cross-section $\sigma_{ex}(\nu_L + \nu_{S1})$ where ν_{S1} is the pure electronic S_0–S_1 transition frequency and the triangle shows the measured T_1 triplet–triplet absorption cross-section $\sigma_T(\nu_L)$. The structural formula of eosin Y is included.

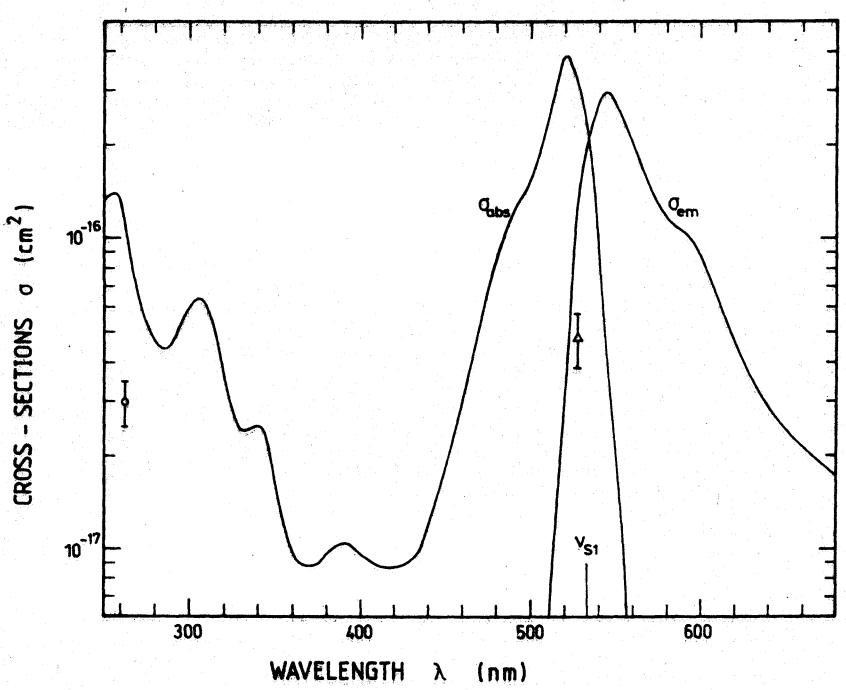

Fig. 6. Absorption cross-section and stimulated emission cross-section spectra of eosin Y in methanol. $\sigma_{ex}(\nu_L + \nu_{S1})$ and $\sigma_T(\nu_L)$ are indicated as circle and triangle, respectively.

The purified dye was dissolved in either methanol (absolute analytical grade) or water (bidistilled, pH ≈ 7). The absorption cross-section spectra and the stimulated emission cross-section spectra of the solutions are shown in figs. 5 (H_2O) and 6 (methanol). In fig. 5 the absorption spectrum of chromatographically purified eosin Y in H_2O is included for comparison (from ref. [53]). The difference in the absorption cross-section spectra is thought to be caused by the presence of fluorescein derivatives with a lower degree of bromination [6,54–56] in our recrystallized dye.

5. Experimental results

The experimental energy transmission $T_{E,L1}$ of the first pump pulse through eosin Y in H_2O (circles) and in methanol (triangles) is shown versus pump pulse peak intensity in fig. 7. The small signal transmission of the dyes was set to $T_0 = 0.01$ at the laser wavelength ($\lambda_L = 527$ nm). At high input peak intensities the absorption bleaching saturates because of S_1–S_n excited state absorption. The triplet-state absorption plays no role in the transmission of the first pump pulse since the pulse duration Δt_L is too short and the intersystem-crossing rate k_{isc} is too slow to cause an appreciable triplet state population (see fig. 3).

The experimental energy transmission ratios $T_{E,L2}/T_{E,L1}$ of the second to the first pump pulse versus input peak intensity I_{0L} ($I_{0L} = I_{0L1} \simeq I_{0L2}$) are displayed by the circles in fig. 8(a) and (b) for eosin Y in H_2O and methanol, respectively. The transmission ratio is influenced by the quantum yield of triplet formation ϕ_T, the T_1–T_n triplet–triplet absorption cross-section σ_T, and the T_n–T_1 triplet–triplet relaxation time τ_T (see fig. 3).

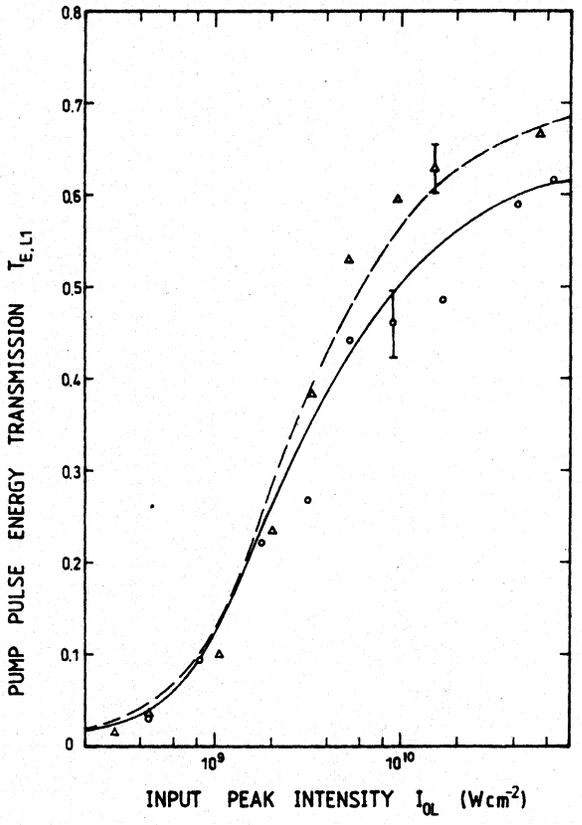

Fig. 7. Energy transmission $T_{E,L1}$ of first pump pulse through sample. Circles and solid curve, eosin Y in H_2O. Triangles and dashed curve, eosin Y in methanol. Small signal transmission is $T_0 = 0.01$. The curves are calculated with the parameters of table 2. σ_{ex} is adjusted to fit the energy transmission at high pump pulse intensities. Curves are independent of ϕ_T, σ_T and τ_T.

The experimental energy transmission $T_{E,P1}$ of the first delayed probe pulse versus pump pulse peak intensity is displayed by the circles in fig. 9(a) and (b) for eosin Y in H_2O and methanol, respectively. Since the delay time t_D (= 8 ns) is long compared to the fluorescence lifetime τ_{S1}, the singlet system is fully relaxed and the intersystem-crossing to the triplet system is completed. Without intersystem-crossing to the triplet system the delayed probe pulse transmission $T_{E,P1}$ should be equal to the small signal transmission T_0 (see fig. 2). The increased probe pulse transmission is determined by the quantum yield of triplet formation ϕ_T and the smaller triplet–triplet absorption cross-section σ_T compared to the singlet ground-state absorption cross-section σ_L.

The experimental probe pulse transmission ratios $T_{E,P2}/T_{E,P1}$ versus I_{0L} are shown by the circles in fig. 10(a) and (b). Without intersystem-crossing it would be $T_{E,P2}/T_{E,P1} = 1$ (see fig. 2). At a fixed quantum yield of triplet formation ϕ_T the ratio $T_{E,P2}/T_{E,P1}$ rises with decreasing σ_T (see fig. 3). An imperfect spatial overlap of the pump and probe pulses in the sample would lower the $T_{E,P2}/T_{E,P1}$ ratio. For high pump pulse peak intensities a focusing to the sample was necessary which made an accurate overlap of the pump and probe pulses difficult. Therefore no experimental data are shown at high pump pulse intensities ($I_{0L} \gtrsim 2 \times 10^9$ W/cm^2).

6. Numerical simulations

In the numerical simulations (equation system (1)–(8)) the quantum yield of triplet formation ϕ_T (eq. (14)), the S_1–S_n excited state absorption cross-section σ_{ex}, the T_1–T_n triplet–triplet absorption cross-section σ_T, and the T_n–T_1 triplet–triplet relaxation time τ_T are determined. The fixed dye parameters for the calculations together with the determined parameters are collected in table 2.

The absorption cross-section data are taken from figs. 5 and 6. The fluorescence quantum yields ϕ_F, the radiative lifetimes τ_{rad}, and the S_1-state lifetimes τ_{S1} (eq. (13)) have been determined from fluorescence quantum distribution measurements (see section 4.2). The Franck–Condon relaxation time τ_{FC} [57] and the S_n–S_1 relaxation times τ_{ex} [58] are assumed. The reorientation times τ_{or} are taken from ref. [59]. The reported phosphorescence lifetime τ_P of eosin Y in H_2O [28,51,60–65] vary between 1.98

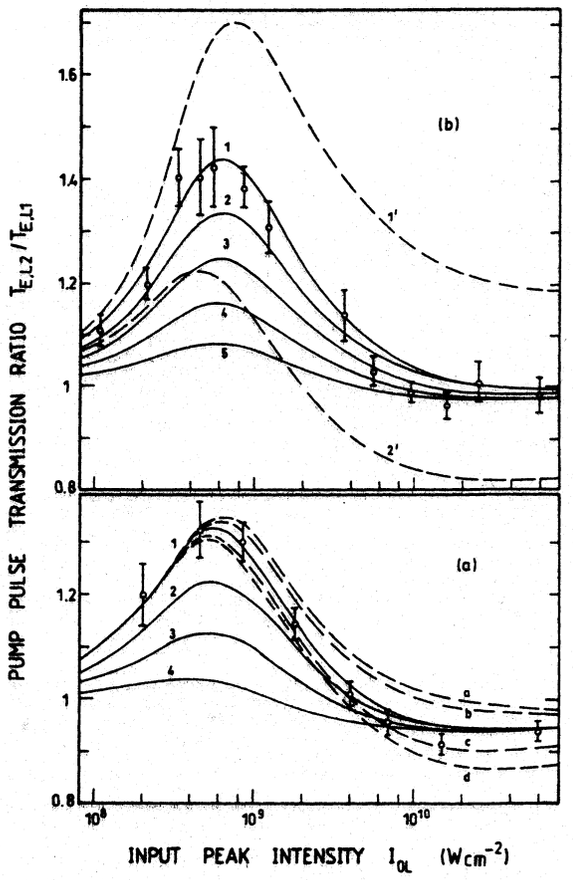

Fig. 8. Energy transmission ratio of pump pulses $T_{E,L2}/T_{E,L1}$ versus input pump pulse peak intensity. The circles are the experimental points. The curves are calculated using the parameters of table 2. (a) Eosin Y in H_2O. Solid curves: τ_T is fixed to 1 ps. (1) $\phi_T = \phi_{T,max} = 1 - \phi_F = 0.8$ and $\sigma_T = 5\times10^{-17}$ cm^2; (2) $\phi_T = 0.6$ and $\sigma_T = 5.2\times10^{-17}$ cm^2; (3) $\phi_T = 0.4$ and $\sigma_T = 6\times10^{-17}$ cm^2; (4) $\phi_T = 0.2$ and $\sigma_T = 8\times10^{-17}$ cm^2. Dashed curves: $\phi_T = 0.8$ and $\sigma_T = 5\times10^{-17}$ cm^2 with $\tau_T = 20$ ps (a), 5 ps (b), 0.3 ps (c) and 0.1 ps (d). (b) Eosin Y in methanol. Solid curves: τ_T is fixed ot 1 ps. (1) $\phi_T = \phi_{T,max} = 1 - \phi_F = 0.56$ and $\sigma_T = 4.5\times10^{-17}$ cm^2; (2) $\phi_T = 0.45$ and $\sigma_T = 4.7\times10^{-17}$ cm^2; (3) $\phi_T = 0.35$ and $\sigma_T = 5.1\times10^{-17}$ cm^2; (4) $\phi_T = 0.25$ and $\sigma_T = 5.8\times10^{-17}$ cm^2; (5) $\phi_T = 0.15$ and $\sigma_T = 7.1\times10^{-17}$ cm^2. Dashed curves: $\tau_T = 1$ ps and $\phi_T = 0.56$ with (1′) $\sigma_T = 0$, and (2′) $\sigma_T = 1\times10^{-16}$ cm^2.

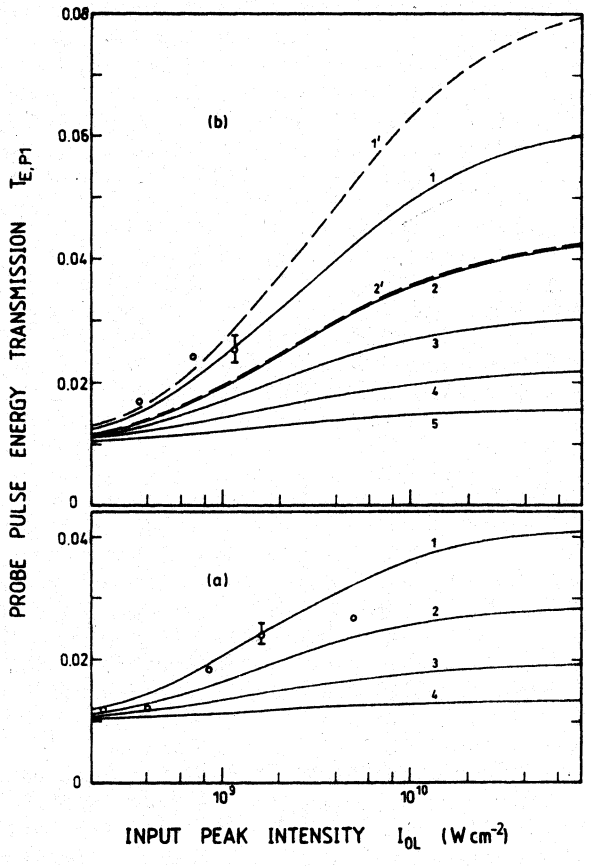

Fig. 9. Energy transmission of first probe pulse through eosin Y in H_2O (a) and eosin Y in methanol (b). Delay time $t_D = 8$ ns. Probe pulse intensities are kept low that they themselves do not change the population distribution measurably. The circles are the experimental points and the curves are calculated. The same parameters as in fig. 8 are applied. Curves are independent of τ_T (dashed curves a–d of fig. 8(a) coincide with solid curve 1).

μs [28] and 2.38 ms [62]. For our studies the exact value of τ_P is without influence because τ_P is much longer than our maximum observation time of $t_R + t_D$.

In fig. 7 σ_{ex} is adjusted to fit the experimental pump pulse transmission $T_{E,L1}$ at high intensities. The best fitting σ_{ex}-values are listed in table 2.

The energy transmission ratio $T_{E,L2}/T_{E,L1}$ in fig. 8(a) and (b) depends on ϕ_T, σ_T and τ_T. For the displayed solid curves ϕ_T is varied, τ_T is fixed to 1 ps, and σ_T is adjusted to fit approximately the experimental data at pump pulse intensities around $I_{0L} = 4 \times 10^{10}$ W/cm^2. For the dashed curves in fig. 8(a) τ_T is varied ($\phi_T = 0.8$, $\sigma_T = 5 \times 10^{-17}$ cm^2). For $I_{0L} \gtrsim 2 \times 10^{10}$ W/cm^2 the rising experimental transmission ratio indicates transient absorption bleaching in the triplet state system. The slopes of the calculated curves fit best to the experimental data for a triplet–triplet relaxation time of 0.3 ps $< \tau_T <$ 1.5 ps. For the dashed curves in fig. 8(b) σ_T is varied. σ_T influences strongly the transmission ratio around $I_{0L} = 2 \times 10^{10}$ W/cm^2. In this intensity region σ_T is fitted. Around $I_{0L} = 5 \times 10^8$ W/cm^2 the transmission ratio depends strongly on ϕ_T. There this value is fitted. The best fitting parameters of ϕ_T, σ_T, and τ_T are collected in table 2. The quantum yield of internal conversion $\phi_{ic} = 1 - \phi_T - \phi_F$, the internal conversion rate k_{ic} (eq. (15)), and the intersystem-crossing rate k_{isc} (eq. (14)) are included in table 2.

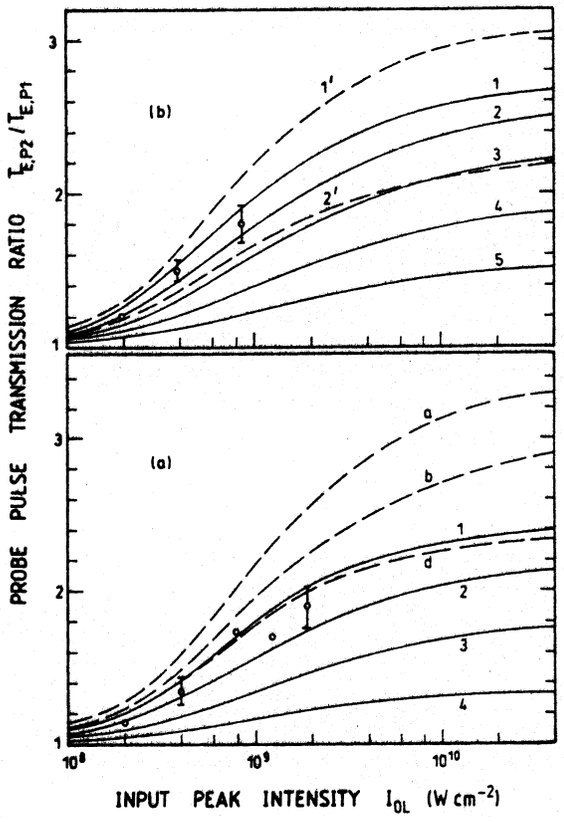

Fig. 10. Energy transmission ratio of probe pulses $T_{E,P2}/T_{E,P1}$ for eosin Y in H_2O (a) and eosin Y in methanol (b). Circles are experimental points and curves are calculated. The same parameters as in fig. 8 are applied. In (a) curve c would be between curve 1 and curve d (not shown for clarity).

Table 2
Spectroscopic parameters of eosin Y used in the simulations. Wavelength $\lambda_L = 527$ nm. room temperature ($\vartheta = 293$ K).

Parameter	Solvent H_2O	References	Solvent Methanol	References
Fixed dye parameters used in simulations				
σ_1 (cm^2)	2.2×10^{-16}	Fig. 5 and [53]	3.2×10^{-16}	Fig. 6
τ_{S1} (ns)	0.95	This work and [47,70] [a]	2.0 [a]	This work
τ_{rad} (ns)	4.73	This work and [46,47]	4.63	This work and [45]
τ_{FC} (ps)	0.7	Assumed [57]	0.7	Assumed [57]
τ_{ex} (ps)	0.06	Assumed [58]	0.06	Assumed [58]
τ_{or} (ps)	550	[59]	330	[59] [b]
τ_P (μs)	190	[64]	172	[45]
ϕ_F	0.2	This work and table 1	0.44	This work and table 1
$\Delta\tilde{\nu}_{23}$ (cm^{-1})	0	Fig. 5 ($\Delta\nu_{23} = \nu_L - \nu_{S1}$)	240 cm^{-1}	Fig. 6
Determined data				
ϕ_T	0.8 ± 0.08		0.56 ± 0.07	
ϕ_{ic}	$\leqslant 0.1$		$\leqslant 0.11$	
k_{isc} (s^{-1})	$(8.4\pm0.8)\times10^8$		$(2.8\pm0.35)\times10^8$	
k_{ic} (s^{-1})	$\leqslant 1.05\times10^8$		$\leqslant 5.5\times10^7$	
σ_{ex} (cm^2)	$(4.5\pm0.5)\times10^{-17}$		$(3\pm0.5)\times10^{-17}$	
σ_T (cm^2)	$(5.5\pm1)\times10^{-17}$		$(4.9\pm1)\times10^{-17}$	
τ_T (ps)	1 ± 0.5		1 ± 0.5	

[a] see also refs. [12] and [44].
[b] calculated by use of relation $\tau_{or}(\text{methanol}) = \tau_{or}(H_2O)\eta(\text{methanol})/\eta(H_2O)$ where the dynamic viscosities are $\eta(\text{methanol}) = 0.6$ cP and $\eta(H_2O) = 1.0$ cP [59].

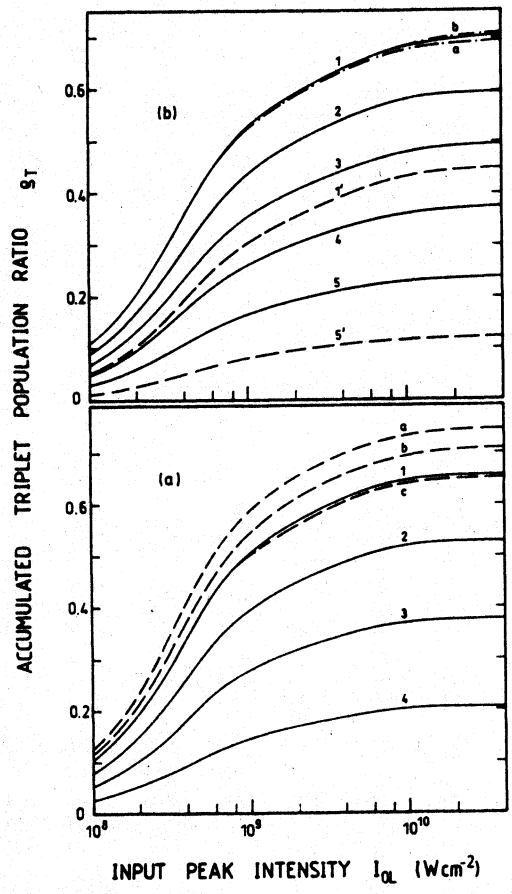

Fig. 11. (a) Accumulated triplet population ratio $\rho_{T2} = \int_0^l \bar{N}_5(t_D + t_R, z', r = 0)\, dz'/N_0 l$ for eosin Y in H_2O. Solid curves $\tau_T = 1$ ps with $\phi_T = 0.8$ and $\sigma_T = 5\times10^{-17}$ cm^2 (1), $\phi_T = 0.6$ and $\sigma_T = 5.2\times10^{-17}$ cm^2, $\phi_T = 0.4$ and $\sigma_T = 6\times10^{-17}$ cm^2 (3), $\phi_T = 0.2$ and $\sigma_T = 8\times10^{-17}$ cm^2 (4). Dashed curves, $\phi_T = 0.8$ and $\sigma_T = 5\times10^{-17}$ cm^2 with $\tau_T = 20$ ps (a), 5 ps (b) and 0.1 ps (c). (b) Accumulated triplet population ratios ρ_{T1} ($t' = t_D$, dashed curves) and ρ_{T2} ($t' = t_R + t_D$, solid curves) for eosin Y in methanol. The varied parameters are (1,1') $\phi_T = 0.56$ and $\sigma_T = 4.5\times10^{-17}$ cm^2, (2) $\phi_T = 0.45$ and $\sigma_T = 4.7\times10^{-17}$ cm^2, (3) $\phi_T = 0.35$ and $\sigma_T = 5.1\times10^{-17}$ cm^2, (4) $\phi_T = 0.25$ and $\sigma_T = 5.8\times10^{-17}$ cm^2, (5,5') $\phi_T = 0.15$ and $\sigma_T = 7.1\times10^{-17}$ cm^2. Dash-dotted curves ρ_{T2} for $\phi_T = 0.56$ with $\sigma_T = 0$ (a) and $\sigma_T = 1\times10^{-16}$ cm^2 (b).

The first probe pulse energy transmission $T_{E,P1}$ is displayed in fig. 9. $T_{E,P1}$ is independent of τ_T. The dependence on σ_T is indicated by the dashed curves in fig. 9(b). The probe pulse transmission ratio $T_{E,P2}/T_{E,P1}$ is shown in fig. 10. The influences of τ_T and σ_T on $T_{E,P2}/T_{E,P1}$ are shown by the dashed curves in fig. 10(a) and (b), respectively. The best fitting values of fig. 8 gives good fits in the figs. 9 and 10.

The accumulation of the dye molecules in the triplet state is illustrated in fig. 11. The triplet level population depends on the time t' after excitation, the spatial position z along the sample (because of pump intensity reduction along the sample length), and on the radial position r across the pump laser beam profile. The triplet level populations $\bar{N}_5$ at the probe pulse positions t_D and $t_R + t_D$ for $r = 0$ are averaged over the sample length ($\int_0^l \bar{N}_5(z')\, dz'/l$) and normalized to the total dye number density N_0 to give $\rho_{T1} = \int_0^l \bar{N}_5(t' = t_D, z', r = 0)\, dz'/N_0 l$ and $\rho_{T2} = \int_0^l \bar{N}_5(t' = t_R + t_D, z', r = 0)\, dz'/N_0 l$.

In fig. 11(a) $\rho_{T2}(I_{0L})$ curves are shown for various quantum yields of triplet formation ϕ_T (solid curves, $\tau_T = 1$ ps) and for various triplet–triplet relaxation times τ_T (dashed curves, $\phi_T = 0.8$). The solvent is water.

In fig. 11(b) the solvent is methanol. The dashed curves show normalized triplet level populations $\tau_{T1}(I_{0L})$, for two ϕ_T values, while the solid curves show normalized triplet level populations $\rho_{T2}(I_{0L})$ for various ϕ_T values. The dash-dotted curves ($\phi_T = 0.8$, $\tau_T = 1$ ps, σ_T varied) indicate that the accumulation of molecules in the triplet state is nearly independent of σ_T.

For our situations of $\phi_T(H_2O) \simeq 0.8$ and $\phi_T(\text{methanol}) \simeq 0.56$ we determined triplet population ratios of $\rho_{T2}(H_2O) \simeq 0.65$ and $\rho_{T2}(\text{methanol}) \simeq 0.53$ at high pump pulse intensities ($I_{0L} \gtrsim 4 \times 10^{10}$ W/cm^2).

7. Discussion

The quantum yields of triplet formation determined in our picosecond two-pulse triplet accumulation studies are in agreement with most of the previously reported data (see table 1). In the solvents H_2O and methanol the radiative lifetimes τ_{rad} are approximately the same. The internal conversion rates k_{ic} in H_2O and methanol are negligibly small compared to the intersystem-crossing rates k_{isc}.

A triplet–triplet absorption cross-section of $\sigma_T = 1.07 \times 10^{-16}$ cm^2 at $\lambda = 518$ nm has been reported for eosin Y in H_2O [26]. Our value of σ_T (H_2O, 527 nm) $\simeq 5.5 \times 10^{-17}$ cm^2 is approximately a factor of two smaller. Data on σ_{ex} and τ_T have not been found in the literature.

8. Conclusions

A two-pulse-sequence picosecond saturable absorption technique has been described which allows the determination of the quantum yield of triplet formation, the singlet excited-state absorption cross-section, the triplet absorption cross-section, and the triplet–triplet relaxation time. Already the pump pulse transmissions $T_{E,L1}$ and $T_{E,L2}$ provide all information. In our studies the probe pulse transmissions were measured to confirm the pump pulse results.

The technique may be applied to triplet accumulation studies of many dyes. A detailed knowledge of the quantum yield of triplet formation is a prerequisite of quantitative triplet–triplet spectroscopy.

Acknowledgements

The work was supported by the Commission of the European Communities Directorate-General for Science, Research and Development in an International Coorporation with the Technion-Israel Institute of Technology in Haifa (professor Sh. Speiser). The authors thank the Rechenzentrum of the Universität Regensburg for allocation of computer time.

References

[1] P.N. Marshall, Histochem. J. 10 (1978) 1.
[2] D. Wittekind, in: Standardization and Quantitation of Diagnostic Staining in Cytology, eds. M.E. Born and L.P. Kok (Coulomb Press Leyden, London, 1986) Ch. 3, p. 30.
[3] M. Koizumi, S. Kato, N. Magata, T. Matsuura and Y. Usui, Photosensitized Reactions (Kagakudojin Publishing Co., Kyoto, 1978).
[4] H.H. Wasserman and R.W. Murray, Singlet Oxygen (Academic Press, New York, 1979).
[5] P. Murasecco-Suardi, E. Gassmann, A.M. Braun and E. Oliveros, Helv. Chem. Acta 70 (1987) 1760.
[6] F. Amat-Guerri, M.M.C. López-González, R. Martinez-Utrilla and R. Sastre, Dyes and Pigments 12 (1990) 249.
[7] P.P. Sorokin, J.R. Lankard, V.L. Moruzzi, IBM J. Res. Dev. 11 (1967) 130.

[8] F.P. Schäfer, Angew. Chem. 82 (1970) 25.
[9] J.R. Lidholt and W.W. Wladimiroff, Opto-Electron. 2 (1970) 21.
[10] M. Maeda, Laser Dyes (Academic Press, London, 1984) p. 101.
[11] A.V. Deshpande and N.B. Iyer, Chem. Phys. Lett. 157 (1989) 239.
[12] A.V. Deshpande and N.B. Iyer, J. Lumin. 46 (1990) 339.
[13] Y. Silberberg and I. Bar-Joseph, Opt. Commun. 39 (1981) 265.
[14] K.P.B. Moosad, T.M. Abdul Rasheed and V.P.N. Nampoori, Opt. Engin. 29 (1990) 47.
[15] K.P.B. Moosad, T.M. Abdul Rasheed, V.P.N. Nampoori and K. Sathianandan, Appl. Opt. 29 (1990) 449.
[16] S. Speiser and D. Dantsker, J. Appl. Phys. 66 (1989) 61.
[17] I. Carmichael and G.L. Hug, J. Phys. and Chem. Reference Data 15 (1986) 1.
[18] V.E. Korobov and A.K. Chibisov, Russ. Chem. Rev. 52 (1983) 27.
[19] K.H. Drexhage, in: Dye Lasers, ed. F.P. Schäfer, 3rd Ed., Top. in Appl. Phys. 1 (Springer, Berlin, 1990) p. 155.
[20] J.B. Birks, Photophysics of Aromatic Molecules (Wiley Interscience, London, 1970).
[21] Mlle. Boudin, J. Chim. Phys. 27 (1930) 285.
[22] C.A. Parker and C.G. Hatchard, Trans. Faraday Soc. 57 (1961) 1894.
[23] C.A. Parker, in: The Triplet State, A.B. Zahlan (Cambridge University Press, Cambridge, 1967) p. 372.
[24] M. Nemoto, H. Kokubun and M. Koizumi, Bull. Chem. Soc. Jpn. 42 (1969) 1223.
[25] A.H. Adelman and G. Oster, J. Am. Chem. Soc. 78 (1956) 3977.
[26] P.G. Bowers and G. Porter, Proc. Roy. Soc. (London) A299 (1967) 348.
[27] K. Gollnick and G.O. Schenck, Pure Appl. Chem. 9 (1964) 507.
[28] M.A. Ryan, E.C. Fitzgerald and M.T. Spitler, J. Phys. Chem. 93 (1989) 6150.
[29] B. Soep, A. Kellmann, M. Martin and L. Lindqvist, Chem. Phys. Lett. 13 (1972) 241.
[30] H.E. Lessing, A. von Jena and M. Reichert, Chem. Phys. Lett. 42 (1976) 218.
[31] A. Penzkofer and W. Falkenstein, Opt. Quant. Electron. 10 (1978) 399.
[32] A. Penzkofer and W. Blau, Opt. Quant. Electron. 15 (1983) 325.
[33] G. Grönninger and A. Penzkofer, Opt. Quant. Electron. 15 (1983) 325.
[34] L.S. Goldberg and P.E. Schoen, IEEE J. Quantum Electron. QE-20 (1984) 628.
[35] D. von der Linde, O. Bernecker and A. Laubereau, Opt. Commun. 2 (1970) 215.
[36] F. Zernike and J.E. Midwinter, Applied Nonlinear Optics (Wiley, New York, 1973).
[37] V.G. Dimitriev, G.G. Gurzadyan and D.N. Nikogosyan, Handbook of Nonlinear Optical Crystals, Springer Series in Opt. Sciences, Vol. 64 (Springer, Berlin, Heidelberg, 1991) p. 65.
[38] A. Penzkofer and W. Falkenstein, Optics Commun. 17 (1976) 1.
[39] A. Penzkofer and W. Leupacher, J. Lumin. 37 (1987) 61.
[40] E.D. Cehelnik, K.D. Mielenz and R.A. Velapoldi, J. Res. Nat. Bur. Stand. Phys. and Chem. 79A (1975) 1.
[41] R. Sens, Dissertation, Universität Siegen (1984).
[42] W. Bäumler and A. Penzkofer, Chem. Phys. 140 (1990) 75.
[43] S.J. Strickler and R.A. Berg, J. Chem. Phys. 37 (1962) 814.
[44] J.B. Birks and D.J. Dyson, Proc. Roy. Soc. (London) A275 (1963) 135.
[45] K. Gollnick, in: Adv. in Photochem., Vol. 6, eds. W.A. Noyes Jr., G.S. Hammond and J.N. Pitts Jr. (Wiley Interscience, New York, 1968) p. 2.
[46] P.G. Seybold, M. Gouterman and J. Callis, Photochem. Photobiol. 9 (1969) 229.
[47] G. Porter, E.S. Reid and C.J. Tredwell, Chem. Phys. Lett. 29 (1974) 469.
[48] G.R. Fleming, A.W.E. Knight, J.M. Morris, R.J.S. Morrison and G.W. Robinson, J. Am. Chem. Soc. 99 (1977) 4306.
[49] O.G. Peterson, J.P. Webb, W.C. McColgin and J.H. Eberly, J. Appl. Phys. 42 (1971) 1917.
[50] A.V. Deshpande, A. Beidoun, A. Penzkofer and G. Wagenblast, Chem. Phys. 142 (1990) 123.
[51] T. Ohno, S. Kato and M. Koizumi, Bull. Chem. Soc. Jpn. 39 (1966) 232.
[52] G. Jones II and S. Chatterjee, J. Phys. Chem. 92 (1988) 6862.
[53] E. Zipfel, J.-R. Grezes, W. Seiffert and H.W. Zimmermann, Histochemistry 74 (1982) 539.
[54] P.N. Marshall, Histochem. J. 8 (1976) 487.
[55] E. Gandin, J. Piette and Y. Lion, J. Chromatogr. 249 (1982) 393.
[56] B.M. Van Liedekerke and A.P. De Leenheer, J. Chromatogr. 528 (1990) 155.
[57] Penzkofer, W. Falkenstein and W. Kaiser, Chem. Phys. Lett. 44 (1976) 82.
[58] F. Graf and A. Penzkofer, Opt. Quantum. Electron. 17 (1989) 53.
[59] G.R. Fleming, J.M. Morris and G.W. Robinson,Chem. Phys. 17 (1976) 91.
[60] V. Kasche and L. Lindqvist, Photochem. Photobiol. 4 (1965) 923.
[61] G.J. Fischer, C. Lewis and D. Madill, Photochem. Photobiol. 24 (1976) 223.
[62] E.F. Zwicker, J. Phys. Chem. 67 (1963) 549.

[63] A.G. Kepka and L.I. Grossweiner, Photochem. Photobiol. 14 (1971) 621.
[64] A. Seret, E. Gandin and A. van de Vorst, Chem. Phys. Lett. 135 (1987) 427.
[65] F. Rizutto and J.D. Spikes, Photochem. Photobiol. 25 (1977) 465.
[66] M. Nemoto, K. Kokubun and M. Koizumi, Bull. Chem. Soc. Jpn. 42 (1969) 2464.
[67] E. Hey and K. Gollnick, Int. Conf. on Photochemistry, Munich, 6–9 Sept. 1967, Reprints Part II, p. 465.
[68] P. Pringsheim, Fluorescence and Phosphorescence (Wiley Interscience, New York, 1949).
[69] O.S. Khalil, Mol. Photochem. 8 (1977) 399.
[70] W.-Z. Lin, Y.-L. Zhang and X.-D. Fang, in: Picosecond Phenomena III, eds. K.B. Eisenthal, R.M. Hochstrasser, W. Kaiser and A. Laubereau, Springer Series in Chem. Phys. Vol. 23 (Springer, Berlin, 1982) p. 282.